

# New Physical Methods for a Space Resolved Mapping of the Macroscopic Polarisation in Molecular Crystals and a Stochastic Theory for Understanding

Jürg Hulliger\*

**Abstract:** The spatial distribution of polarity in molecular crystals built up by dipolar entities was imaged by two new techniques: Scanning pyroelectric microscopy (SPEM) and phase-sensitive second harmonic microscopy (PS-SHM). SPEM maps the variation in electrical polarisation due to a change in temperature (pyroelectric effect). The PS-SHM contrast is caused by a change of the sign of the molecular hyperpolarisability (nonlinear optical effect). A spatial inhomogeneity of polar properties in molecular crystals is predicted by a 2D Ising-type model describing 180° orientational disorder at the crystal–nutrient interface. As a result of (slow) growth, centric and acentric seed crystals can continuously transform into bipolar (twinned) crystals showing an inhomogeneous spatial distribution of polarity in the as-grown state.

**Keywords:** Orientational disorder · Phase sensitive second harmonic microscopy · Polar domains · Scanning pyroelectric microscopy · Stochastic theory

## 1. Introduction

In general, tensorial properties [1] of molecular crystals [2] describing effects of *electrical polarity* arise from acentric arrangements of whatever the molecular entities are. Whereas an acentric packing of *centric molecules* results mostly in weak macroscopic effects of polarity, crystals grown from *dipolar molecules* featuring a strong nonlinear electrical polarisability can show pronounced polar properties [3]. Effects of macroscopic polarity in molecular crystals may be due to (i) a ferroelectric or ferroelastic phase [4], or (ii) be the result of simply adding up tensorial (uneven rank) properties of molecules [3]. In view of the large number of solved crystal structures, we know that only a few examples of ferroelectric and ferroelastic organic crystals of neutral

molecules exist [4][5]. Therefore, most of the crystals investigated for their polar properties are materials where *dipolar* entities are packed such as to represent a *piezoelectric* or a *pyroelectric* symmetry class.

In the case of ferroelectric and ferroelastic materials (i), *domain* formation is typical and has mainly been investigated by polarised light microscopy and dielectric measurements [4][5]. For the second, the main class (ii) of acentrically packed dipolar molecules, a spatially *homogeneous* distribution of polarity in single component materials is expected, however, for crystals showing none of the types of mechanical twinning [6]. Up to this point, we have briefly summarised some of the classical views.

During the last few years we have been developing a new theory [7–9] and corresponding experimental techniques [10–12] in order to understand and visualise *as-grown inhomogeneities* of the spatial distribution of polarity (length scale:  $\mu\text{m}$  to  $\text{mm}$ ) in different kinds of molecular crystals (see Table).

Essentially, we have introduced a *stochastic process of orientational disorder* (180° flips of dipoles) taking place at the crystal–nutrient interface (Fig. 1). Approaching real interfaces by a nutrient

and an adlayer (thermalised) on top of a bulk structure (non thermalised), configurational entropy ( $\Delta S_{\text{defect}} > 0$ ) allows for a certain density of 180° faulted ( $\Delta E_{\text{defect}} > 0$ ) dipole orientations ( $\downarrow$  vs  $\uparrow$ ) within the adlayer.

As a result of growth, the polar or nonpolar state of a seed initially formed by a process of nucleation may undergo changes. For the purpose of further discussion and experimental investigation, we shall distinguish two cases:

1. Centric and piezoelectric point groups which do not allow for a *vector* property.
2. Pyroelectric point groups which allow for a *vector* property.

*Case 1:* Grown-in orientational defects may turn *e.g.* *centric* packings of seed single-crystals into objects showing macroscopically large domains. On average, the symmetry of growth sectors (domains) affected by the stochastic process [7–9], belongs always to a *pyroelectric* group, because the process of disorder preserves a vector property at the growing interface.

*Case 2:* For growth along the inequivalent directions of the unique axis in pyroelectric symmetry classes, we intuitively may expect to obtain a different density of faulted molecular orientations,

\*Correspondence: Prof. Dr. J. Hulliger  
Department of Chemistry and Biochemistry  
University of Bern  
Freiestr. 3  
CH–3012 Bern  
Tel.: +41 31 631 42 41  
Fax: +41 31 631 39 93  
E-Mail: juerg.hulliger@iac.unibe.ch

Table. Examples of materials showing a stochastic effect of polarity

Crystalline host materials	Comments on guests and properties
Perhydrotriphenylene (PHTP) [13]	Many D-, A-type dipolar molecules have been included. SHG, SPEM and PS-SHM
Thiourea [14]	Reports on the inclusion of dipolar guests. SHG
1,8-bis((1)-adamantyl)-1,3,5,7-octatetrayne [15]	2-butanon and long-chain NLO guests. SHG and SPEM
Triphenylphosphacene [16]	Inclusion of many D-, A-type guests. SHG
Phthalic acid [17]	Stained crystals, e.g. by para-nitroaniline, showed SHG to be due to inclusion of dyes in some sectors.
Several types of single component organic crystals [18] X-ray: centric structure	Showed weak SHG indicative of disorder or solid solution formation with impurities giving rise to polarity.
Solid solutions $A_{1-x}B_x$ of organic molecules showing shape similarity [19]	SHG effects for $A_{1-x}B_x$ , A: centric lattice of symmetrical molecules enriched by a dipolar species B.

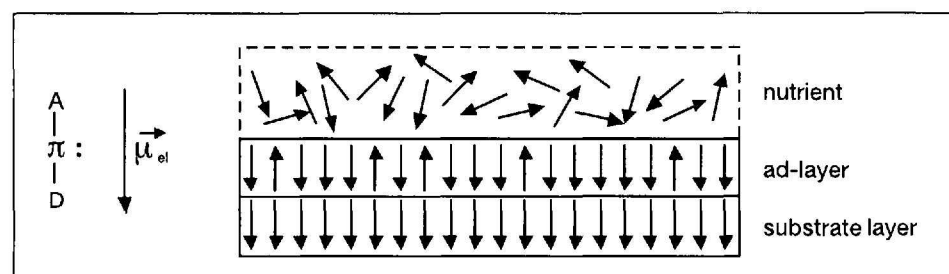


Fig. 1. Schematic representation of a homogeneous substrate (where dipoles do not relax) with an attached adlayer (where relaxation is allowed), containing dipoles oriented either  $\downarrow$  or  $\uparrow$  (molar fractions  $X_A(\downarrow)$ ,  $X_D(\uparrow)$ , correspondingly). Dipoles in the nutrient shall have no preferred orientation.

which would give rise to a different degree of reduction of the polar properties with respect to the two directions of growth. However, here the stochastic theory predicts that along one of the polar directions we will have faulted orientations as discussed, whereas along the other direction, growth and defect formation may give rise to a  $180^\circ$  flip of the *majority* of dipoles. After this growth-induced transition has taken place, growth in both directions of the former polar axis produces an equal density of defects. Whether this flip takes place for a crystal of a finite length or not, depends on the molecular couplings involved [20]. A summary of the behaviour for cases 1 and 2 is provided by Fig. 2.

Phenomena as predicted by the theory reviewed above present challenges for experimental techniques to investigate polar properties of organic crystals. Within the crystallographic community, researchers may at first consider advanced diffraction techniques by using

e.g. micro-beamline synchrotron facilities, including methods of anomalous scattering. A spot-wise resolution of the crystal structure (averaged over the volume of diffraction) may indeed provide information on the spatial distribution of the degree of polar ordering, including the sign of polarity – although the method is very elaborate.

In collaboration with solid-state physicists (Dr. M. Wübbenhorst, Delft University and Dr. M. Flörshemer, Münster University) we have developed two independent methods which provide a spatial mapping of the polarity to a resolution in the range of *micrometers*: (i) Scanning pyroelectric microscopy (SPEM) [10][11], and (ii) phase sensitive second harmonic microscopy (PS-SHM) [12]. In Sections 2 and 3 we give a brief review on these techniques. In Section 4 we provide more details on the stochastic theory, including numerical examples for a realistic estimation of the degree of disorder issued for experimental investigations.

## 2. Scanning Pyroelectric Microscopy (SPEM)

In the thermally and mechanically unperturbed state, the intrinsic polarisation  $P$  of a pyroelectric crystal at ambient conditions is compensated by outer charges distributed over the polar faces. Charge compensation can be disturbed by a rapid change in temperature producing e.g. excess surface charges due to the pyroelectric

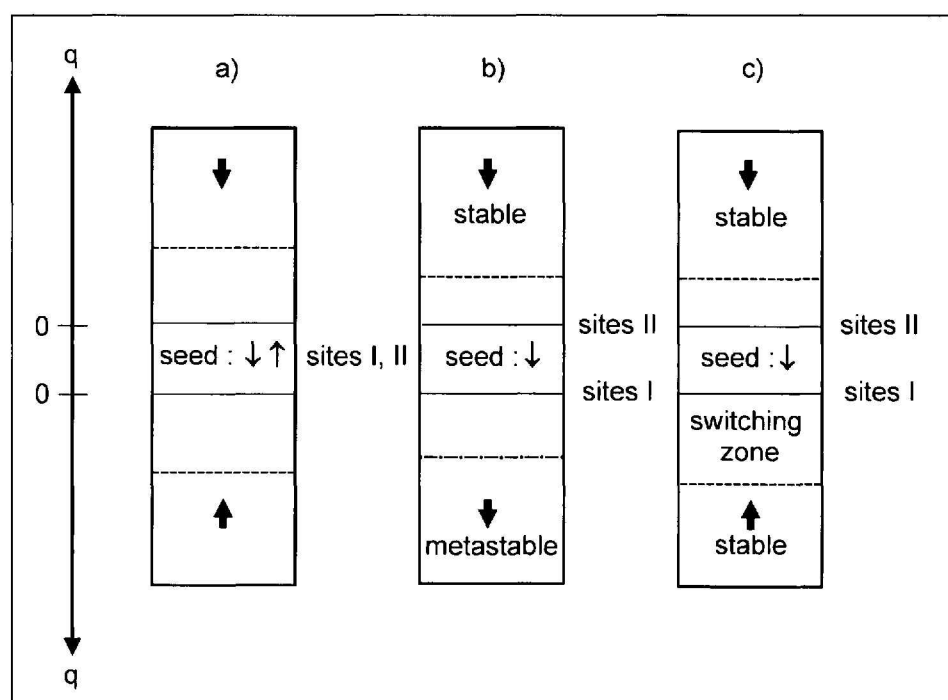


Fig. 2. Graphical representation of the state of polarity after a large number of attachments to a seed providing perfect centric (a) or acentric (b, c) ordering. For details see text and [9].

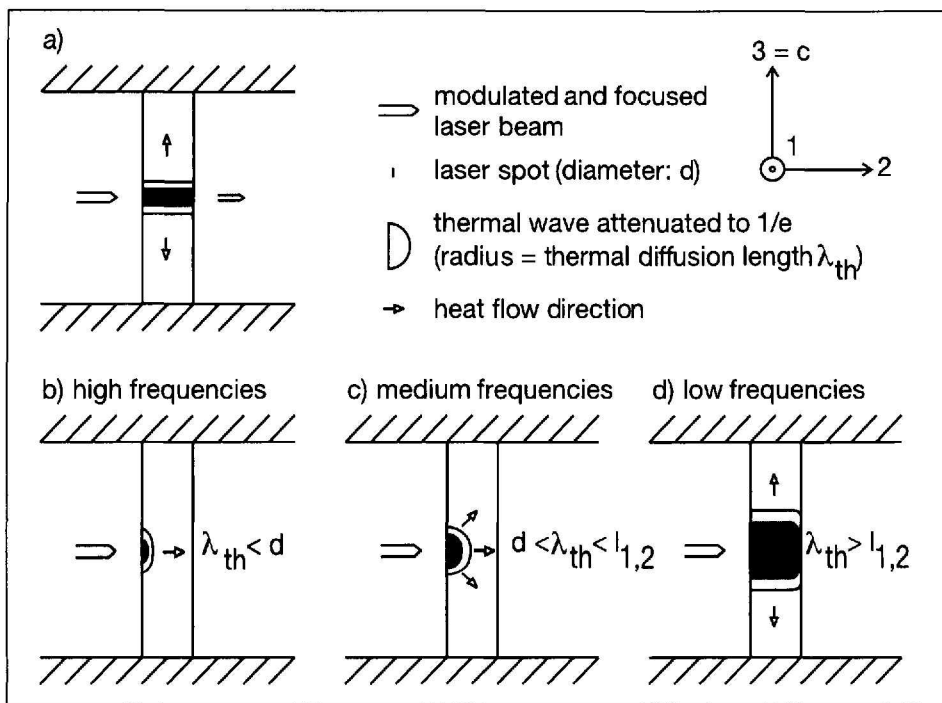


Fig. 3. Four special cases of heat transport in a needle-like sample between two plate electrodes: (a) heat absorption in the volume  $\Rightarrow$  1D heat flow along the needle axis; (b-d) heat generation in a thin insulating absorption layer on the crystal surface. Changing frequencies from high to low, the heat flow direction changes from (i) perpendicular to the needle axis, to (ii) semispherical heat propagation (medium frequencies), to (iii) 1D heat flow in the needle 3-direction, similar to case (a).

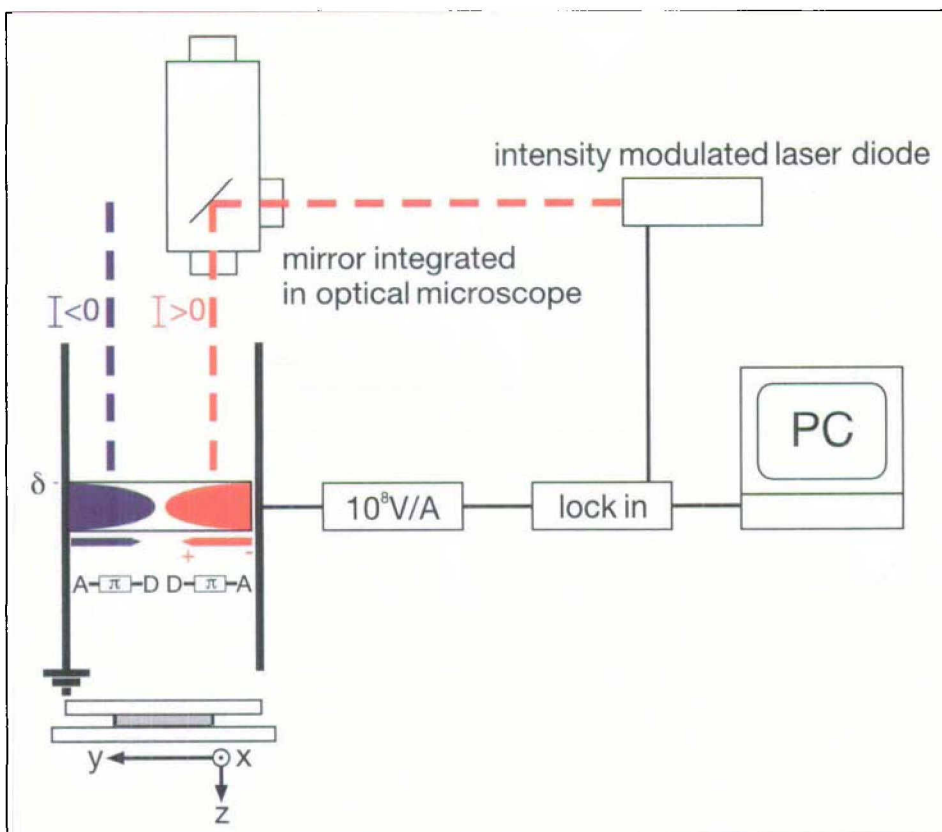


Fig. 4. Experimental setup for SPEM. As indicated, the sample consists of two areas of opposite polarisation. Heating samples (locally) in either domain of polarisation, opposite excess charges result on both capping faces, *i.e.* at electrodes. This induces a discharge current flowing through the outer circuit. Depending on the heated domain, the current direction is either positive or negative.

effect [1]. A mapping of the 2D polarisation distribution in a material is possible if the intensity modulated beam of a laser diode scans over the sample surface. Provided that light is absorbed within a surface layer, the excitation creates a temperature change which is described by a thermal wave propagating perpendicular to the surface. Its penetration depth is given by  $\lambda_{th} = \sqrt{K/\pi f}$ ,  $K$  being the thermal diffusivity and  $f$  the modulation frequency. Given a certain  $K$ , information on polarisation in the third dimension, the depth, can be gained at low  $f$  (a few Hz), whereas a near to surface response is obtained at high  $f$  (a few hundreds of Hz). For more details on the propagation of heat in needle-like crystals, see Fig. 3. The lateral resolution in *surface*-SPEM is limited by the laser spot size (presently a few  $\mu\text{m}$ ) [21]. An experimental setup is shown in Fig. 4. For a surface mode analysis, crystal surfaces were coated by an insulating black pigment. Samples were placed between two plate electrodes contacted with silver paste on the low (-) side, thermally and mechanically separated by an air gap from the high (+) side of the high sensitive input of electronics [10].

*Tomographic* information was obtained by layered thinning of crystals [11]. SPEM was applied in the analysis of the spatial distribution of the polarisation in zeolite [15] and inclusion materials [10][11]. In the case of channel-type inclusion compounds of perhydrotriphenylene (PHTP), SPEM was the first technique able to reveal (i) the bipolar structure, and (ii) the cone-shaped distribution of polarity, as predicted by computer simulations based on a Markov model (see Section 4, model (1)).

In Fig. 5 a series of SPEM images shows the  $(x,y)$ -distribution of the pyroelectric response of prismatic faces thinned down in steps to reach the middle part, where seeding took place (red pixels: positive current; blue pixels: negative current). The colour intensity is hence a measure of the local polarisation strength (lateral resolution:  $\sim 20 \mu\text{m}$ , probed layer thickness:  $\sim 10 \mu\text{m}$ ). White spots represent areas of vanishing polarisation.

Because of the measured sign of the current and the assumption that  $dP/dT < 0$  (supported by the fact, that in PHTP/NPP (NPP = 1-(4-nitrophenyl)piperazine) thermal expansion is the main contribution to the pyroelectric effect [10]), we know that *acceptor groups* (such as  $-\text{NO}_2$ ) are predominantly directed towards the crystal surface. This finding is in agreement with the prediction of a



Markov model, assuming a strong repulsion between collinearly arranged  $O_2N$ -groups. The cone-like evolution of polarity is seen in Fig. 5d, where SPEM was measured in the middle of the crystal. Further details on the spatial distribution of the polarisation in PHTP inclusion compounds were obtained by means of a thermal wave analysis [23].

### 3. Phase-Sensitive Second Harmonic Microscopy (PS-SHM)

Optical *second* harmonic generation (SHG) can be observed in acentric crystals [3]. Optical nonlinearity is described by *e.g.* a third-rank tensor given by elements  $d_{ijk}$ . Conditions for nonzero coefficients result from the transformation behaviour of  $d$  under the symmetry elements of the point group [1]. In the case of molecular crystals where macroscopic polarity results mainly from the acentric packing of polar molecules,  $d$  is proportional to the sum over the molecular hyperpolarisability  $\beta_{ijk}$ , distributed over the crystal lattice. Given a coordinate system of a crystal, and molecules featuring essentially a  $\beta_{zzz}$  (charge transfer contribution) element, there is a change of the sign of  $\beta_{zzz}$  for molecules related by inversion symmetry. In order to match

most simple conditions for domain mapping, crystals should show a thickness (in the direction of the fundamental wave propagation) below the coherence length  $l_c$  for SHG:

$$l_c = \lambda_0 / 4(n_{10} - n_{20}) \quad (1)$$

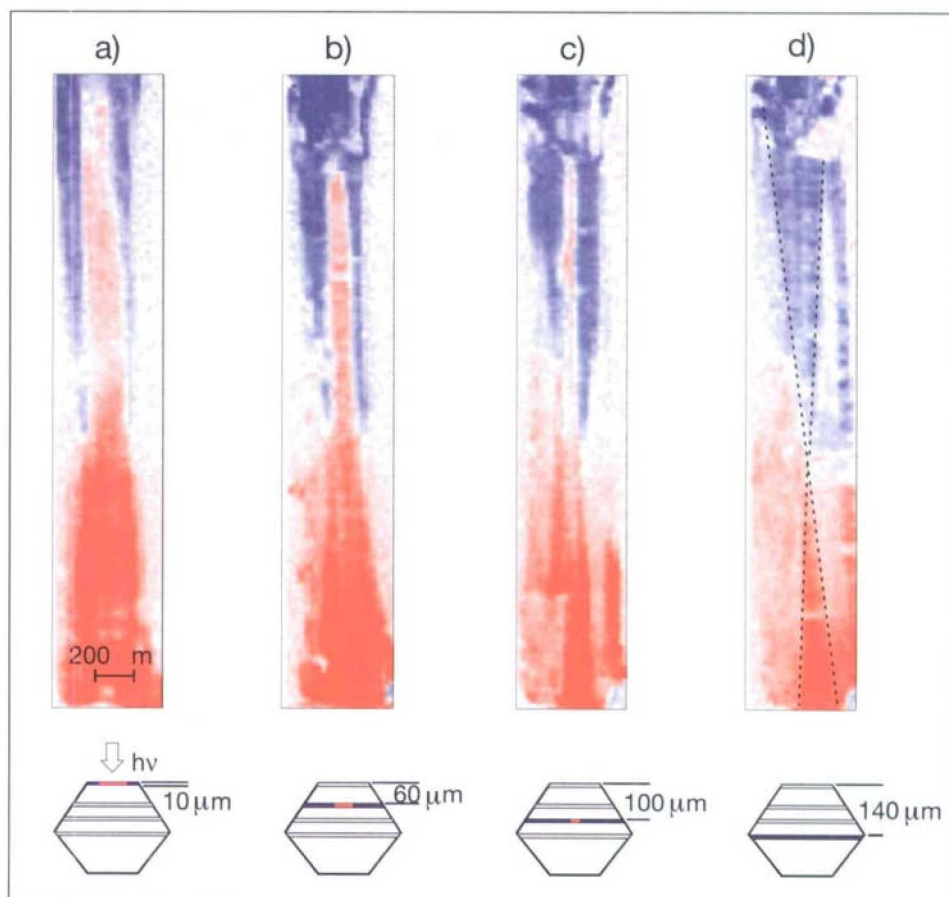
Using a fundamental wavelength of  $\lambda = 1064$  nm and organic materials with a typical optical dispersion of the refractive index [3], present second harmonic microscopy can work on the basis of plate- or needle-like crystals of a thickness in the range of a few micrometers or less. Such samples may be produced by edge-defined melt growth in-between glass plates or from solution growth using evaporation on glass slides (eventually assisted by a spin coating technique) [12]. Working with small objects can be advantageous, because the growth of small and perfect crystals of complex molecular materials is often more successful than growing larger ones. A scheme of the SHM setup is shown in Fig. 6.

A first attempt at gaining information with SHM is by the investigation of the polarisation dependence of the SHG response from platelets, which ideally feature a polar axis parallel to the supporting glass substrate. In this respect, channel-

type inclusion compounds showed clearly that the dominant contribution to the SHG response results from a polarisation of the fundamental wave parallel to the channel axis  $c$ . Along this axis the Markov process (model (1), Section 4) produces polarity in two adjacent macrodomains in which the direction of the resultant polarisation is either  $\uparrow$  or  $\downarrow$ . In the normal mode of SHM, there is no way to see that the crystal is bipolar, as predicted by the Markov model. However, this important information can be obtained by *phase-sensitive* second harmonic microscopy (PS-SHM). The optical principle of its operation is shown in Fig. 7.

Provided that the crystal thickness is in the range or below  $l_c$ , a reference beam of a polarised SH wave will undergo a constructive or destructive interference with a SH wave generated by the sample itself. By adjusting the phase difference between the fundamental and the SH reference wave, all parts of our bipolar crystals with the correct sign of  $d$  allowing constructive interference will appear bright, whereas the adjacent domain will release a SH signal of much lower intensity (ideally zero). Keeping all optical settings constant, but rotating the crystal around an angle of  $180^\circ$  ( $\perp$  to the incident beam), will interchange the brightness of the macrodomains where either enhanced

Fig. 5. SPEM images of a PHTP/1-(4-nitrophenyl)piperazine single crystal thinned down by four steps. The position dependent pyroelectric response  $p_3(x, y)$  at a constant frequency  $f = 415$  Hz is shown for all layers. Colour code: red = positive current, blue = negative current, white = zero current. Step size:  $20 \mu\text{m}$ . Current range:  $-0.2 \text{ pA} \leq I_{\text{pyro}} \leq 0.2 \text{ pA}$ .





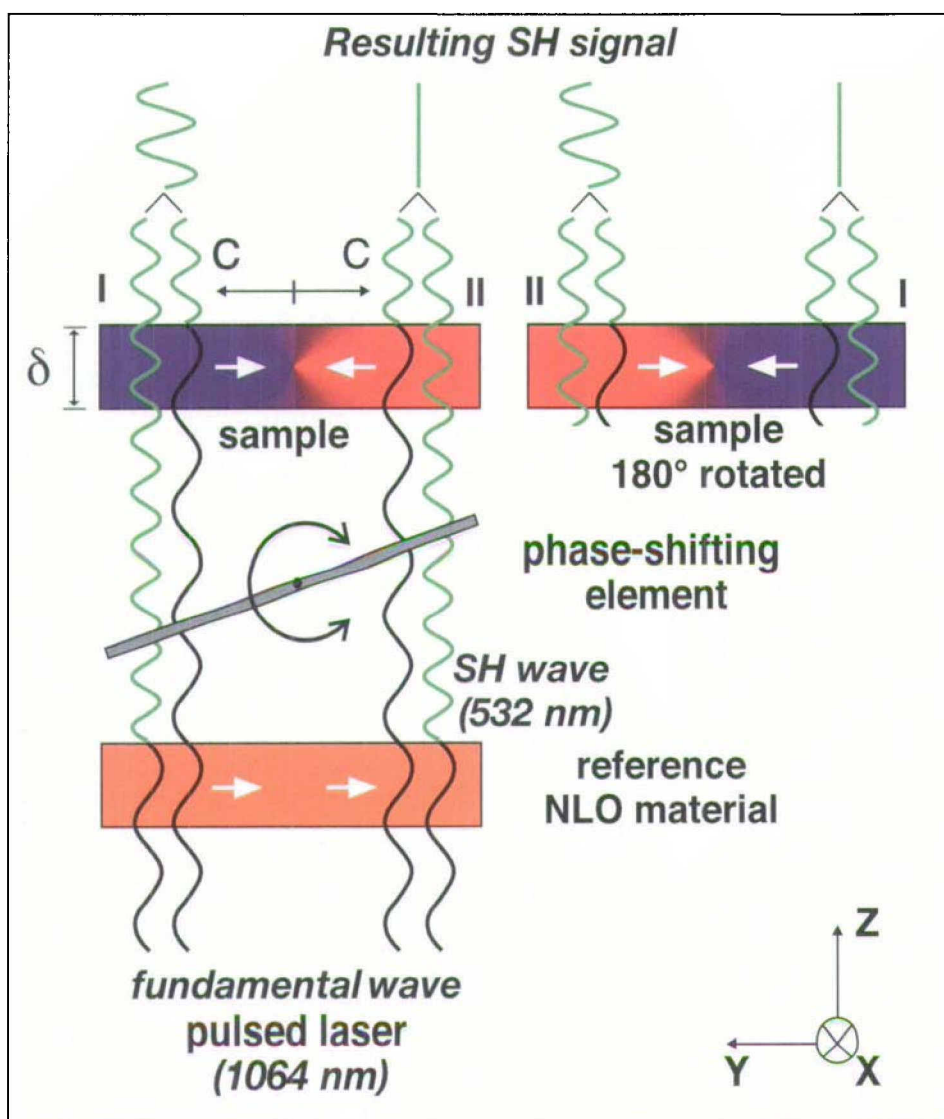


Fig. 6. Schematic principle of far-field phase-sensitive SH microscopy (PS-SHM). Oppositely orientated domains (coloured blue and red) in a sample with a uniform thickness  $\delta$  emit SH light with a phase shift of  $\pi$ . Domain contrast is achieved by using the interference effect between the sample and a homogeneous SHG reference plate (the white arrows refer to the polarity direction). An angle-tuned glass plate allows the phase to be adjusted between the (polarised) fundamental waves and the SH waves from the reference plate in order to reach maximum intensity, e.g. at the 'blue' side of the sample. Keeping optical settings constant but rotating the sample by  $180^\circ$  leads to an interchange of contrast: maximum intensity at the 'red' side. The arrows (x, y, z) indicate the laboratory coordinate system.

or attenuated SH waves are released. For more details and references to optical principles, see [12].

A first example is shown in Fig. 8: Here, PS-SHM reveals the bipolar structure of crystals of a perhydrotriphenylene inclusion compound. If compared to SPEM (Section 2), PS-SHM allows the mapping of the spatial distribution of the polarisation in the optical far field limit and without contacting samples with electrodes. Because of the transmission mode, no *tomographic* information is provided so far. However, if we would operate in a *reflectance mode*, surfaces of small and particularly large crystals would become accessible to this technique.

In addition to qualitative characterisation of new materials, PS-SHM turned out to be extremely useful in determining the absolute polarity of domains if a reference thin crystal of known polarity is used. Here, we encounter a clear advantage over X-ray crystallography, which can deduce such information by analysis of anomalous scattering properties.

#### 4. Elements of and Predictions by the Stochastic Theory on Polarity

##### 4.1. Definitions

From a topological point of view our layer by layer growth process (Section 1), which accounts for orientational disorder within the adlayer, may be described by a 2D Ising effective spin model. In this notation, three independent parameters describing interaction energies enter the formalism.

A most simple parameterisation is given by dipolar-type molecules terminated on either side by acceptor (A)- and donor (D)-type fragments setting up short range intermolecular couplings such as  $-A \cdots A-$  ( $E_{AA}$ ),  $-D \cdots D-$  ( $E_{DD}$ ) and  $-A \cdots D-$  ( $E_{AD}$ ), where points represent the interaction. Lateral short range interactions to neighbours may be due to  $\uparrow \cdots \uparrow$  ( $E_p$ ),  $\uparrow \cdots \downarrow$  ( $E_{ap}$ ) and a coordination number  $z_\perp$ . For more details, see [9]. Effectively, we define three energy differences being the basic parameters approaching real binding networks in crystals by a minimum set of parameters:  $\Delta E_A = E_{AA} - E_{AD}$ ,  $\Delta E_D = E_{DD} - E_{AD}$ ,  $\Delta E_\perp = E_p - E_{ap}$ .

##### 4.2. Levels of Description

Because there is no exact solution for the 2D Ising system in non-zero field, we have elaborated a number of approximate analytical solutions along with numerical Monte Carlo simulations:

- 1) Markov chain model, exact solution for  $\Delta E_\perp = 0$ , perturbational solution for small lateral coupling [8][9].
- 2) Schottky-type model for a low number of defects in acentric or centric crystals [7].
- 3) Markov chain models, taking into account the effect of  $\Delta E_\perp$  [20].
- 4) Bethe-Peierls model for an effective two-layer system [24].
- 5) Monte Carlo simulations using a  $100 \times 100$  grid, closed boundary conditions and a layer by layer thermalisation [20].

(Models (3) to (5) were developed in collaboration with H. Bebie, Bern University.)

To get an idea to which materials these models may apply, we have to make a comment on the nature of channel-type inclusion lattices and lattices representing solid solutions of organic



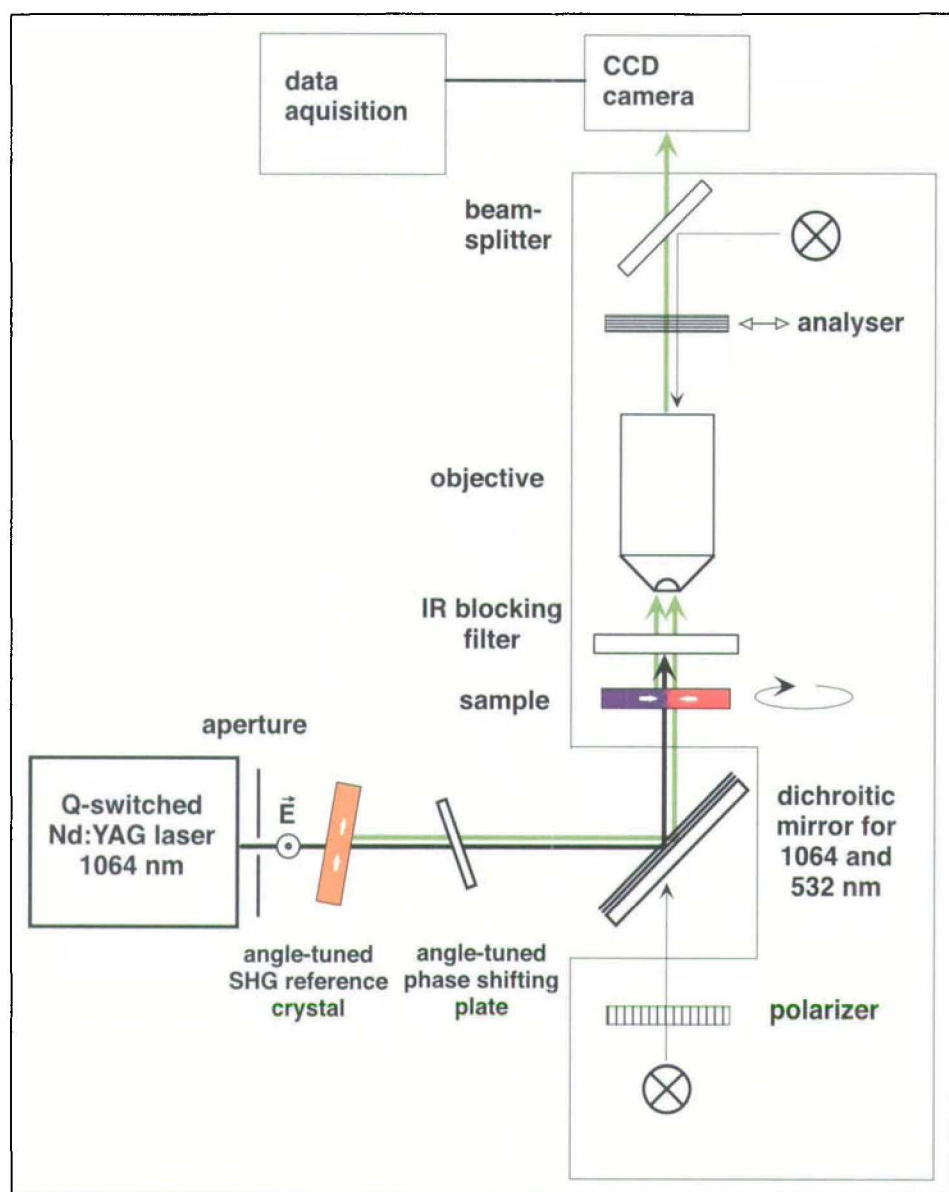


Fig. 7. Schematic setup of a far-field phase-sensitive SH microscope (PS-SHM).

molecules. Let us group real materials into classes where (i)  $|\Delta E_{\perp}| \leq 0 - 0.5$  kJ/mol and (ii)  $|\Delta E_{\perp}| > 0.5$  kJ/mol at 300 K. In class (i) the lateral interaction has a minor effect on net polarity, whereas in (ii) the coupling between the effective spins is significantly influenced or even dominated by  $\Delta E_{\perp}$ .

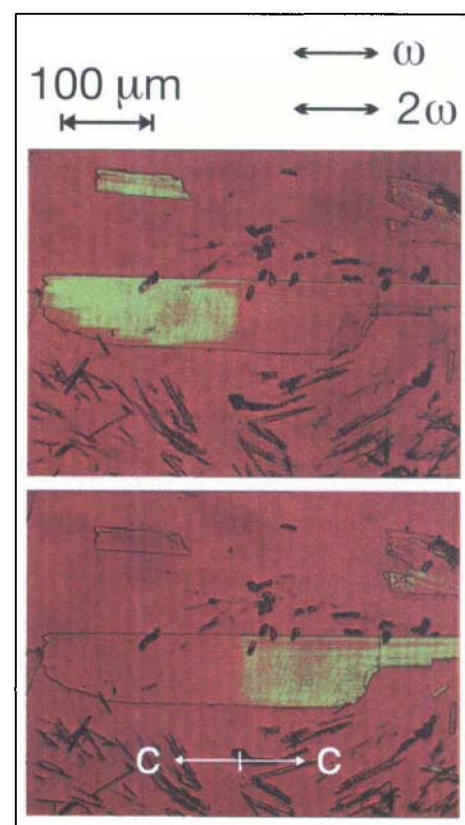
Examples for both classes can be found among inclusion compounds and solid solutions. Kitogorodski was the first to recognise the analogy between solid-solution formation and orientational defects in organic crystals [25]. In accordance to criteria for solid solution formation in organic crystals, molecules should not differ more than about 20% in their geometrical similarity. For continuous solubility it is necessary that the energy surfaces describing the molecular interactions are similar, especially with respect to their deepest minima.

Fig. 8. Domain contrast: visualisation of  $180^{\circ}$  domains. In the upper picture the SH intensity of one domain is enhanced while attenuated within the other. Contrast inversion occurs if the sample is rotated by  $180^{\circ}$ . The lower picture (for comparison rotated by  $180^{\circ}$  with respect to the upper one) shows the opposite sign of the polarity of the other domain. Some thickness variation is apparent. Both pictures represent superpositions of the linear optical image and the SH response (green). In these experiments, the fundamental and the generated SH light are polarised along the crystal c-axis (indicated by arrows) corresponding to the (+ or -)  $d_{\text{eff}}$  element of the second-order hyperpolarisability tensor.

#### 4.3. Results and Predictions

A pictorial summary on the possible behaviour of real organic crystals grown slowly from dipolar molecules is provided by Fig. 9.

At a given temperature  $T$ , realistic  $\Delta E_A$ ,  $\Delta E_D$  values and for a large number of attached layers, the resultant fraction  $X_{\text{net}} \equiv X_A(\downarrow) - X_D(\uparrow)$  is shown for  $-5 \leq \Delta E_{\perp} \leq 5$  kJ/mol ( $z_{\perp} = 4$ , the coordination number in 2D). Basically, there are three ranges of  $\Delta E_{\perp}$  values, namely  $\Delta E_{\perp} < -2.5$  kJ/mol,  $\Delta E_{\perp} > 2.5$  kJ/mol and  $-2.5 \leq \Delta E_{\perp} \leq 2.5$  kJ/mol giving rise to (i) nearly perfect *acentric* order (left side, P), nearly perfect *centric* order (right side, AP) and significant disorder (middle part, P'). Referring to Fig. 2c (Section 1) we show here a case which corresponds to a stable development of polarity for  $\Delta E_{\perp} < 0$ . Note that polarity can exist, although  $\Delta E_{\perp}$  may be small ( $\Delta E_{\perp} > 0$ ) or even zero. This means that all crystals grown from dipolar molecules are expected to show a pyroelectric effect if  $\Delta E_{\perp}$  is smaller than about 2.5 kJ/mol (300 K,  $z_{\perp} = 4$ ). We address here a certain range for  $\Delta E_{\perp}$ , because the  $X_{\text{net}}$  function depends also on  $\Delta E_A$ ,  $\Delta E_D$ . However, Monte Carlo simulations for  $\Delta E_{\perp} > 0$  showed, that irrespective of realistic values for  $\Delta E_A$ ,  $\Delta E_D$  a range for  $\Delta E_{\perp} > 2-3$  kJ/mol is meaningful. In order to have  $X_{\text{net}} \geq 0.05$ ,  $\Delta E / \Delta E_{\perp}$  should be larger or about 5 (for  $\Delta E = \Delta E_A - \Delta E_D > 0$ ,  $z_{\perp} = 4$ ,  $T = 300$  K).



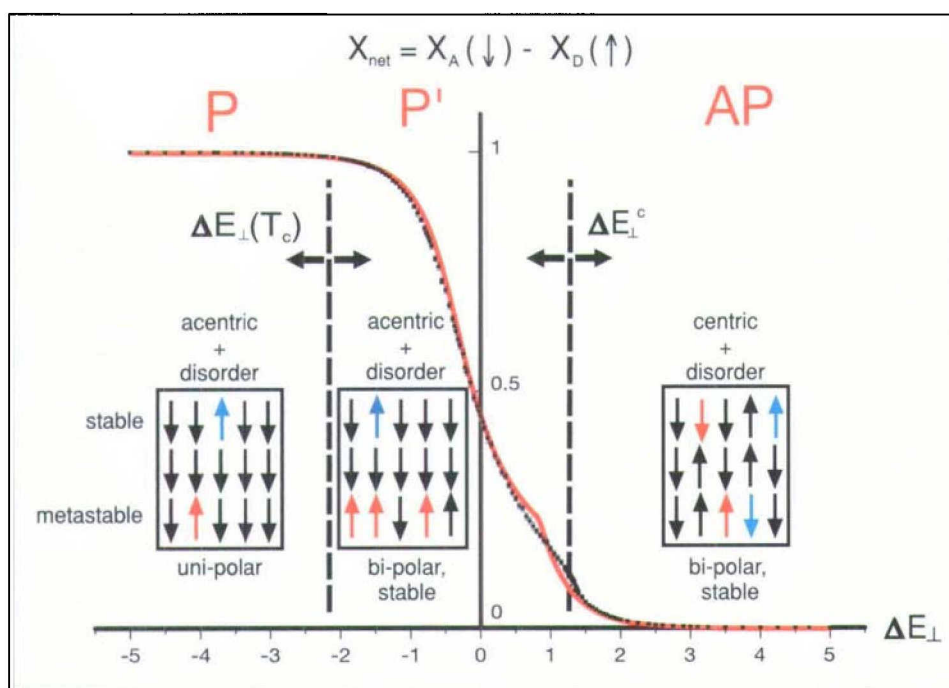


Fig. 9. Influence of the lateral coupling on the net polarity at given values for  $\Delta E_A = 5$  kJ/mol,  $\Delta E_D = 2$  kJ/mol and  $T = 300$  K (grid size  $100 \times 100$ , periodic boundary conditions,  $z_{\perp} = 4$ , kJ/mol). Points: Monte Carlo simulation. Red curve: Markov model taking into account the effect of  $\Delta E_{\perp}$  (see Section 4, model (3)). P: parallel alignment of dipoles, AP: antiparallel, P': parallel, but with significant disorder.

There are additional features provided by Fig. 9: To the *right* side, there is a *phase transition* [24]. Above the transition  $P' \rightarrow AP$  the lattice may be described by a centric packing being perturbed by defects. Below the transition, the packing is more like acentric on average, strongly perturbed by defects unless a negative  $\Delta E_{\perp}$  is more and more turning down disorder.

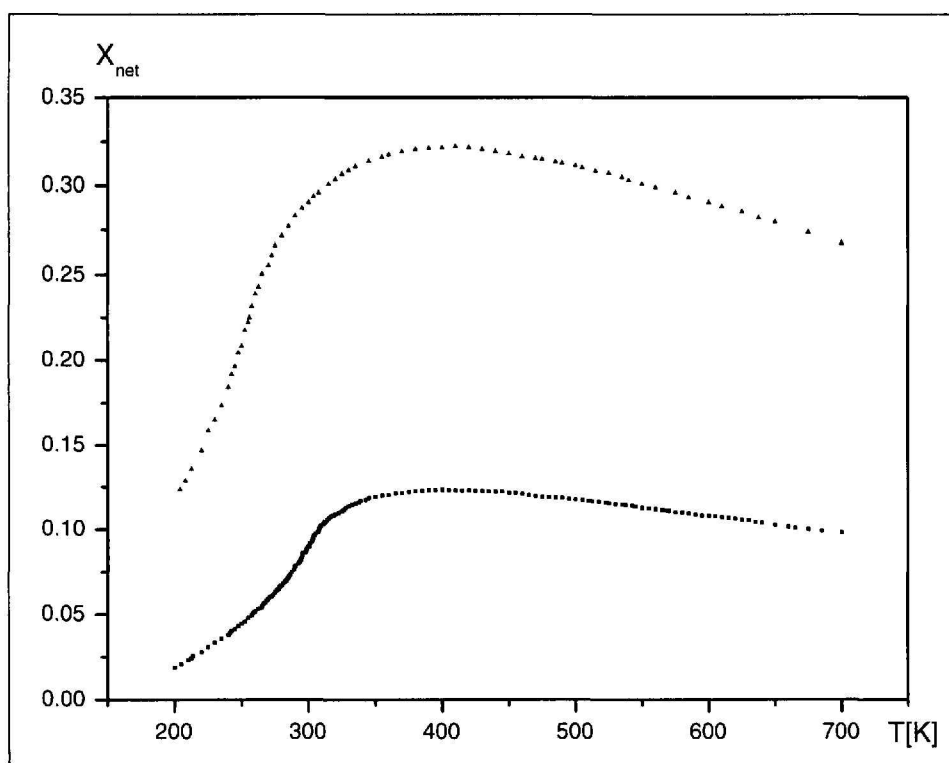
On the *left* side, there is given another limit, however, to be taken as less sharp as to the right side: Close to  $\Delta E_{\perp}^c$ , in one of the polar directions of a *pyroelectric*

group (determined by the sign of  $\Delta E$ ) most of the dipoles will undergo a *switch* when attached as growth proceeds (Fig. 2c). In another context, such a behaviour has been termed a kinetic phase transition [26]. In our case the crystal is undergoing a transition which may need a few to a very large number of attached layers to be completed.

At this point of our analysis, the model is introducing a fundamentally new view on how some organic crystals belonging to a pyroelectric class may undergo a special kind of a stochastic twin-

ning mechanism. In cases where the probability for switching is very low ( $\Delta E_{\perp} \ll \Delta E_{\perp}^c$ ,  $\Delta E_A$  small but larger zero), upper and lower growth sectors along the polar axis will show a different level of Schottky-type orientational defects [7][20].

So far, we have discussed the effect of  $\Delta E_{\perp}$  at constant  $T$ . However we can also experimentally vary  $T$ . By changing the temperature of growth we can hence influence the level of orientational defects in e.g. a 'centric' crystal structure. Because of a similarity to antiferromagnetism, Fig. 10 shows a maximum for  $X_{\text{net}}$  at temperatures for the growth of real materials. As a result of Monte Carlo simulations it is likely to have a few percent in  $X_{\text{net}}$  if  $\Delta E_{\perp}$  is smaller than 2.5 – 5 kJ/mol at temperatures in the range of 300 – 600 K.



## 5. Conclusions

Summarising our theoretical and experimental studies of the last five years on molecular crystals grown slowly from dipolar-type molecules, we can conclude:

- The faulted structure of as-grown materials defined above features, on average, pyroelectric symmetry.
- As a result of growth, faulted crystals belonging to a 'centric' group are

Fig. 10. Temperature dependence of  $X_{\text{net}}$  for given sets of interactions:  $\Delta E_A = 5$  kJ/mol (lower), 10 kJ/mol (upper),  $\Delta E_D = 2$  kJ/mol (both),  $\Delta E_{\perp} = 1.35$  kJ/mol (lower), 1.45 kJ/mol (upper). Monte Carlo simulations (model (5), see Section 4). A maximum of net polarity can be expected for a given material at temperatures which may be below the melting points of single component materials.



twinned. Along polar directions of a non-uniform crystal, there are two domains featuring opposite net polarity.

- As a result of growth, faulted crystals belonging to a 'polar' group may show a switching of the majority of dipoles on one side of the polar direction.
- In the language of a 2D Ising model, defect formation depends on  $\Delta E_A$ ,  $\Delta E_D$  and  $\Delta E_{\perp}$ . In order to have a concentration of faulted orientations larger than or about  $X_{\text{net}} = 0.05$ , conditions with respect to the interactions and temperature are known [20].

In any case, covered by arguments given above, we can expect to find crystals showing an *inhomogeneous spatial distribution of polarity*. Two different techniques, SPEM and PS-SHM were developed to investigate these fundamental properties at first in the case of channel-type inclusion compounds. Technical improvement is presently directed to increase the sensitivity of PS-SHM in order to see minor effects of disorder resulting in polar crystalline sectors of single component materials assigned to centric space groups by X-ray crystallography.

It would be of greatest interest to us if crystallographers would also look out for  $180^\circ$  orientational disorder by means of their sophisticated diffraction techniques and models for the interpretation of diffuse scattering.

### Acknowledgements

Numerous collaborators have contributed to results reviewed here: Dr. M. Wübbenhorst, Dr. A. Quintel, Dr. P. Rechsteiner, Prof. H. Bebie, F. Budde, M. Alaga-Bogdanovic, T. Hertzsch, Dr. S. Kluge and H. Süss. I am indebted to Dr. A. Quintel for arranging the manuscript. Part of this work was supported by NFP 'Functional Supramolecular Materials' (4047-057476/1).

Received: March 30, 2001

- [1] a) J.F. Nye, 'Physical Properties of Crystals', Oxford University Press, Oxford, 1985; b) P. Paufler, 'Physikalische Kristallographie', Akademie-Verlag, Berlin, 1986.
- [2] a) J.D. Wright, 'Molecular crystals', Cambridge University Press, Cambridge, 1995; b) A.I. Kitaigorodsky, 'Molecular Crystals and Molecules', Academic Press, London, 1973.
- [3] 'Nonlinear Optics of Organic Molecules and Polymers', Eds. H. Singh Nalwa, S. Miyata, CRC Press, Boca Raton, 1997.
- [4] M.D. Hollingsworth, *Curr. Opin. Solid State Mater. Sci.* 1996, 1, 514.
- [5] Y. Kamishina, Y. Akishige, M. Hashimoto, *J. Phys. Soc. Jap.* 1991, 60, 2147.
- [6] 'Modern Crystallography IV: Physical Properties of Crystals', Ed. L. A. Shuvalov, Springer-Verlag, Berlin, 1988.
- [7] a) J. Hulliger, *Z. Kristallogr.* 1998, 213, 441; b) J. Hulliger, *Z. Kristallogr.* 1999, 214, 9.
- [8] a) J. Hulliger, P. Rogin, A. Quintel, P. Rechsteiner, O. König, M. Wübbenhorst, *Adv. Mater.* 1997, 9, 677; b) S.W. Roth, P.J. Langley, A. Quintel, M. Wübbenhorst, P. Rechsteiner, P. Rogin, O. König, J. Hulliger, *Adv. Mater.* 1998, 10, 1543; c) J. Hulliger, P.J. Langley, O. König, S.W. Roth, A. Quintel, P. Rechsteiner, *Pure Appl. Opt.* 1998, 7, 221.
- [9] a) J. Hulliger, S.W. Roth, A. Quintel, in 'Crystal Engineering: From Molecules and Crystals to Materials', Eds. D. Braga *et al.*, Kluwer Academic Publishers, NATO Series C: 538, 1999, p. 349; b) J. Hulliger, S.W. Roth, A. Quintel, H. Bebie, *J. Solid State Chem.* 2000, 152, 49.
- [10] A. Quintel, J. Hulliger, M. Wübbenhorst, *J. Phys. Chem. B* 1998, 102, 4277.
- [11] A. Quintel, S.W. Roth, J. Hulliger, M. Wübbenhorst, *Mol. Cryst. Liq. Cryst. A* 2000, 338, 243.
- [12] P. Rechsteiner, J. Hulliger, M. Flörsheimer, *Chem. Mater.* 2000, 11, 3296.
- [13] a) J. Hulliger, O. König, R. Hoss, *Adv. Mater.* 1995, 7, 719; b) R. Hoss, O. König, V. Kramer-Hoss, U. Berger, P. Rogin, J. Hulliger, *Angew. Chem. Int. Ed.* 1996, 35, 1664.
- [14] a) D.F. Eaton, A.G. Anderson, W. Tam, Y. Wang, *J. Am. Chem. Soc.* 1987, 109, 1886; b) W. Tam, D.F. Eaton, J. Calabrese, I. Williams, Y. Wang, A. G. Anderson, *Chem. Mater.* 1989, 1, 128.
- [15] T. Müller, J. Hulliger, W. Seichter, E. Weber, T. Weber, M. Wübbenhorst, *Chem. Eur. J.* 2000, 6, 54.
- [16] a) T. Kobayashi, S. Isoda, K. Kubono, in 'Comprehensive Supramolecular Chemistry 6', Eds. J.L. Atwood, J.E.D. Davies, D.D. Mac Nicol, F. Vögtle, K.S. Suslick, Pergamon Press, Oxford, 1996; b) T. Hertzsch *et al.*, to be published.
- [17] B. Kahr, S.-H. Jang, J.A. Subramony, L. Bastin, M.P. Kelley, *Adv. Mater.* 1996, 8, 941.
- [18] P.J. Langley, J. Hulliger, R. Thaimattam, G.R. Desiraju, *New J. Chem.* 1998, 1307.
- [19] Ongoing work within NFP 'Functional Supramolecular Materials'.
- [20] J. Hulliger, M. Alaga-Bogdanovich, H. Bebie, *J. Phys. Chem. B* 2001, submitted.
- [21] M. Wübbenhorst, J. van Turnhout, G.J. Klap, J.C. Jansen, A. Quintel, J. Hulliger, *IEEE Trans. DEI* 2000, 7, 523.
- [22] G.J. Klap, M. Wübbenhorst, J.C. Jansen, H. van Koningsveld, H. van Bekkum, J. van Turnhout, *Chem. Mater.* 1999, 11, 3497.
- [23] M. Wübbenhorst, J. van Turnhout, A. Quintel, J. Hulliger, *J. Appl. Phys.* 2000, 88, 2108.
- [24] H. Bebie, J. Hulliger, to be published.
- [25] A.I. Kitaigorodsky, 'Mixed Crystals', Springer-Verlag, Berlin, 1984.
- [26] A.A. Chernov, *Sov. Phys. Uspekhi* 1970, 13, 101.